European Journal of Medicinal Chemistry 45 (2010) 5309–5317

Contents lists available at ScienceDirect

European Journal of Medicinal Chemistry

journal homepage: http://www.elsevier.com/locate/ejmech

Original article

Structure-based optimization and biological evaluation of human 20α-hydroxysteroid dehydrogenase (AKR1C1) salicylic acid-based inhibitors

Ossama El-Kabbani [a,*], Peter J. Scammells [a], Tom Day [a], Urmi Dhagat [a], Satoshi Endo [b], Toshiyuki Matsunaga [b], Midori Soda [b], Akira Hara [b]

[a] Medicinal Chemistry and Drug Action, Monash Institute of Pharmaceutical Sciences, Monash University, 381 Royal Parade, Parkville, Victoria 3052, Australia
[b] Laboratory of Biochemistry, Gifu Pharmaceutical University, Daigaku-Nishi, Gifu 501-1196, Japan

ARTICLE INFO

Article history:
Received 22 June 2010
Received in revised form
8 August 2010
Accepted 24 August 2010
Available online 17 September 2010

Keywords:
Aldo-keto reductase
3-Bromo-5-phenylsalicylic acid
Cancer
Drug design
Human 20α-hydroxysteroid dehydrogenase
Human 3α-hydroxysteroid dehydrogenase

ABSTRACT

The tertiary structure of the Leu308Val mutant of human 20α-hydroxysteroid dehydrogenase (AKR1C1) in complex with the inhibitor 3,5-dichlorosalicylic acid (DCL) has been determined. Structures and kinetic properties of the wild-type and mutant enzymes indicate that Leu308 is a selectivity determinant for inhibitor binding. The Leu308Val mutation resulted in 13-fold and 3-fold reductions in the inhibitory potencies of DCL and 3-bromo-5-phenylsalicylic acid (BPSA), respectively. The replacement of Leu308 with an alanine resulted in 473-fold and 27-fold reductions in the potencies for DCL and BPSA, respectively. In our attempts to optimize inhibitor potency and selectivity we synthesized 5-substituted 3-chlorosalicylic acid derivatives, of which the most potent compound, 3-chloro-5-phenylsalicylic acid (K_i = 0.86 nM), was 24-fold more selective for AKR1C1 relative to the structurally similar 3α-hydroxysteroid dehydrogenase (AKR1C2). Furthermore, the compound inhibited the metabolism of progesterone in AKR1C1-overexpressed cells with an IC_{50} value equal to 100 nM.

1. Introduction

Hydroxysteroid dehydrogenases (HSDs) catalyze the synthesis and metabolism of all classes of steroid hormones and play a pivotal role in regulating nuclear receptor signaling by controlling the concentration of active steroid hormones at the pre-receptor level [1,2]. HSDs are broadly classified into two protein superfamilies, the short-chain dehydrogenase/reductase and the aldo-keto reductaseo (AKR) [3,4]. Members of the AKR superfamily are NAD(P)(H)-dependent oxidoreductases that adopt a TIM-barrel motif consisting of a cylindrical core of eight stranded β-sheet surrounded by eight α-helices running antiparallel to the β-sheet [5,6]. While the TIM-barrel motif is well conserved within the family members, it is interrupted by a number of loops and helices of varying lengths. These loops provide the structural variations required for binding chemically diverse substrates and make the enzyme scaffold adaptable to cofactor and/or substrate induced conformational changes [5,7,8]. The cofactor-binding and active sites are conserved across all AKRs where the active site is comprised of a catalytic tetrad which forms an oxyanion pocket along with the nicotinamide ring of the cofactor via a hydrogen bonding network. The reactions catalyzed by AKRs follow an ordered bi–bi kinetic mechanism where the cofactor binds first and leaves last [5,9,10]. Structural studies have shown that significant conformational changes occur in the AKRs upon cofactor-binding resulting in a tight binary complex and a mature substrate binding site [8,11,12].

There are four human NADP(H)-dependent HSDs belonging to the AKR1C subfamily, namely AKR1C1 (20α-HSD), AKR1C2 (type 3 3α-HSD), AKR1C3 (type 2 3α-HSD and type 5 17β-HSD) and AKR1C4 (type 1 3α-HSD), which share over 86% amino acid sequence homology [1,2,8,13]. The AKR1C isoforms have different expression patterns in human tissues, where they regulate ligand occupancy and trans-activation of nuclear receptors by controlling the concentrations of active steroid hormones such as androgens, estrogens and progestins in target tissues [2,13–15]. Although the AKR1C isoforms catalyze the oxidation and reduction reactions with comparable efficiencies, they thermodynamically favor the ketosteroid reduction in vitro [16]. The direction of catalysis in vivo is also governed by the cellular ratio of NADPH/$NADP^+$. In

Abbreviations: HSD, hydroxysteroid dehydrogenase; AKR, aldo-keto reductase; AKR1C1, human 20α-hydroxysteroid dehydrogenase; AKR1C2, human type 3 3α-hydroxysteroid dehydrogenase; *S*-tetralol, *S*-(+)-1,2,3,4-tetrahydro-1-naphthol; $GABA_A$, γ-aminobutyric acid type A; BPSA, 3-bromo-5-phenylsalicylic acid; DCL, 3,5-dichlorosalicylic acid; WT, wild-type; MT, mutant.

* Corresponding author. Tel.: +61 3 9903 9691; fax: +61 3 9903 9143.
E-mail address: ossama.el-kabbani@monash.edu (O. El-Kabbani).

0223-5234/$ – see front matter © 2010 Elsevier Masson SAS. All rights reserved.
doi:10.1016/j.ejmech.2010.08.052

metabolically active cells, reduction is favored over oxidation since NADPH is the predominant form of the cofactor and the dehydrogenase activities of the four isoforms are potently inhibited by NADPH [17,18]. Although the four AKR1C isoforms have overlapping catalytic properties [15], they display distinct positional and stereo preferences for steroid substrates. Differences in affinity for the 3-, 17- or 20-ketosteroid substrates and mode of steroid binding in the active site among the four AKR1C isoforms are dictated by residues lining their substrate binding pockets [2,8,13].

Although AKR1C1 exhibits both 3α/β- and 20α-HSD activities, it preferentially acts as a 20-ketosteroid reductase converting progesterone and its metabolites (5α-dihydroprogesterone and 3α,5α-tetrahydroprogesterone) into the corresponding 20α-hydroxysteroids [17,19–22]. Since the metabolite 20α-hydroxyprogesterone has a low affinity for the progesterone receptors, AKR1C1 plays an important role in controlling the cellular concentration of progesterone, which is an essential hormone required for endometrial development and maintenance of pregnancy [23]. Progesterone is a natural hormone, synthesized in both males and females, and also affects neuronal function by modulating gene expression and cellular receptors abundant in the central nervous system [24]. Progesterone and/or its above metabolites exert neuroprotective effects in traumatic and ischemic brain injury [24], nerve crush injury [25], peripheral neuropathy induced by an antineoplastic agent docetaxel [26], and diabetic neuropathy [27]. In addition, 3α,5α-tetrahydroprogesterone is a potent positive modulator of the $GABA_A$ receptors in the brain [28]. Since AKR1C1 efficiently reduces progesterone and its metabolites, and is ubiquitously expressed in human tissues, its inhibition would lead to elevating the concentrations of neuroactive steroids. On the other hand, the expression of AKR1C1 was reported to be up-regulated in ovarian endometriosis [29], endometrial and breast cancer [30,31], and cancer cells derived from lung and colon [32,33]. Recent work has shown that the enzyme plays a crucial role in induction of neoplastic transformation of NIH3T3 cells [34]. Thus, AKR1C1 is an interesting target for the development of not only new drugs for the treatments of the neurological disorders and endometriosis, but also novel anticancer drugs with pain relief effect through the activation of the $GABA_A$ receptors.

Several classes of AKR1C1 inhibitors have been identified, including, benzodiazepines, benzofurans, phenolphthalein derivatives, benzoyl benzoic acids, steroid carboxylates and *N*-phenylanthranilic derivatives [21,22,35–37]. More recently, we have designed 3-bromo-5-phenylsalicylic acid (BPSA) as a selective and potent inhibitor of AKR1C1 with a K_i value of 4 nM based on the crystal structure of the enzyme in ternary complex with a lead compound [38,39]. Since members of the AKR1C subfamily share high sequence homology and show overlapping substrate specificity, it is important to identify selectivity determinants to aid the development of inhibitors that are specific for AKR1C1. Structural analysis of the inhibitor binding site in the AKR1C1 ternary complex with 3,5-dichlorosalicylic acid (DCL) bound facilitated the identification of nonconserved residues (Leu54, His222, Leu306, and Leu308) involved in hydrogen bonding and van der Waals interactions with the inhibitor. While the amino acid residue Leu308 in AKR1C1 makes van der Waals contacts with both DCL and BPSA, in the other AKR1C isoforms with the exception of AKR1C2 this interaction is not conserved [38,39].

In an effort to investigate the role of Leu308 in inhibitor binding we have examined the effects of the Leu308Val and Leu308Ala mutations in AKR1C1 on the potency of inhibition. A crystal structure of the Leu308Val mutant (MT) enzyme in ternary complex with $NADP^+$ and DCL was determined to identify any structural changes that may have been caused by the mutation in the inhibitor binding site. In addition, the effect of shortening of the Leu308 side-chain on inhibitor binding was investigated by molecular modeling of DCL and BPSA in wild-type (WT) and MT AKR1C1s. Optimization of AKR1C1 inhibitors was carried out where the most potent compound, 3-chloro-5-phenylsalicylic acid (K_i = 0.86 nM), was 24-fold more selective for AKR1C1 over AKR1C2. Furthermore, the compound potently inhibited the metabolism of progesterone by AKR1C1 in the cells with an IC_{50} value of 100 nM.

2. Results and discussion

2.1. Crystal structure of AKR1C1 Leu308Val MT

Crystals of the Leu308Val MT in ternary complex with $NADP^+$ and DCL were obtained by optimizing the salt and precipitant concentrations of the crystallization buffer that was used to crystallize the WT AKR1C1 ternary complex [39]. The final concentrations of zinc sulfate and polyethylene glycol monomethyl ether 550 (PGMME) were reduced from 20 mM to 10 mM and from 25% (v/v) to 15% (v/v) respectively, while keeping the pH (6.5) and the final concentration of MES buffer (0.1 M) unchanged. The asymmetric unit contained one molecule of the Leu308Val MT, one molecule of the cofactor $NADP^+$, one molecule of the inhibitor DCL, 396 solvent molecules, and a zinc ion. The zinc ion from the crystallization buffer was present in coordination with a water molecule, the side-chain of Glu133, and the side-chains of Glu292 and His248 from the

Table 1
Data collection and refinement statistics.

Space group	$P2_1$
Cell dimensions	a = 39.41 Å b = 83.89 Å c = 48.91 Å β = 91.0°
Radiation source	Rotating anode
Wavelength (Å)	1.54178
Diffraction data[a]	
Resolution (Å)	30–1.9
Number of observed reflections	24030 (2377)
Number of unique reflections	22733 (2237)
Redundancy	4.0 (4.8)
Completeness (%)	94.6 (94.1)
$I/\sigma(I)$	11.7 (2.7)
R_{merge} (%)	4.9 (36.0)
Refinement statistics	
Resolution (Å)	30–1.9
Protein residues	318
Solvent molecules	396
Zinc ion	1
Cofactor	1
Inhibitor	1
R_{free} (%)	26.0
R_{cryst} (%)	19.4
RMSDs	
Bonds (Å)	0.022
Angles (°)	2.0
Ramachandran plot	
Residues in most favored regions (%)	93.3
Residues in allowed regions (%)	6.3
Estimated coordinated error	
Luzzati mean coordinate error (Å)	0.244
Mean B factors (Å^2)	
Protein	26.0
$NADP^+$	19.3
Inhibitor	27.5
Water molecules	36.4

[a] Statistics for the highest resolution shell (1.97–1.9 Å) are shown in parentheses.

neighboring symmetry-related molecule. There were 319 amino acids in the final structure that fitted into the electron density map, with the exception of five residues at the N-terminal end. As the electron density was poorly defined for these residues due to disorder in the N-terminus they were omitted from the structural model. The structure was refined to a crystallographic R-factor of 0.194 (R_{free} = 0.260) and during the refinement process, double conformations were assigned to residues Ile49 and Cys242. The root mean square deviations (RMSD) of bond lengths and angles of the refined model were 0.022 Å and 2.0°, respectively. A Ramachandran plot of the backbone torsions had 93.3% of the residues in the most favored region and 6.3% of the residues in the additionally allowed regions [40]. Only Ser221 was in the disallowed region due to the hydrogen bond between its main-chain and the cofactor molecule. A summary of the data collection and refinement statistics is presented in Table 1.

Clear electron density allowed unambiguous fitting of Val308 and the inhibitor molecule into the respective difference Fourier maps (F_o–F_c and $2F_o$–F_c). The RMSD of the MT structure from the WT AKR1C1 was 0.2 Å. As shown in Fig. 1, the Leu308Val mutation did not affect the surrounding residues of the active site except for the side-chain of Phe311 where a change in the torsion angle of the phenyl ring was noticed resulting from the additional interaction with the side-chain of Val308. The key hydrogen bonding interactions between the inhibitor and WT enzyme were conserved in the Leu308Val MT structure. The inhibitor molecule was anchored from its carboxylate group that formed hydrogen bonds with the catalytic residues His117 (2.8 Å) and Tyr55 (2.5 Å), while the hydroxyl group was hydrogen bonded to His222 (3.0 Å). Van der Waals contacts were present between the inhibitor and residues Leu54, Leu306, and Phe311. Unlike the WT enzyme, the side-chain of the mutated Val308 made long contacts with the inhibitor DCL, the closest point of contact being 3.9 Å.

2.2. The role of Leu308 in inhibitor binding

Structural and kinetic studies on the binding of the inhibitors DCL and BPSA to the AKR1C isoforms suggested that the interactions between the inhibitor and the four nonconserved amino acid residues at positions 54, 306, 308, and 311 confer inhibitor selectivity [38,39]. In the case of BPSA, an inhibitor designed based on the structure of AKR1C1 in ternary complex with $NADP^+$ and DCL, its phenyl group targets a nonconserved hydrophobic pocket in the active site of the enzyme lined by residues Leu54, Leu308 and Phe311, resulting in a 21-fold improved potency (K_i = 4 nM) over the structurally similar AKR1C2 [38]. In this study, the contribution of Leu308 in inhibitor binding to AKR1C1 was investigated by mutating Leu308 to valine and alanine residues, and determining the effects of the mutations on the binding constants (K_i values) for DCL and BPSA. The Leu308Val mutation resulted in a 13-fold increase in the K_i value for DCL and a 3-fold increase in the K_i value for BPSA compared to the WT, while in the case of the Leu308Ala MT the K_i values for DCL and BPSA increased by 473-fold and 27-fold, respectively (Table 2).

Table 2
Effects of the mutations of Leu308 in AKR1C1 on K_i values for DCL and BPSA.

Enzyme	K_i (nM)[a]	
	DCL	BPSA
WT	5.9 ± 0.8	4.1 ± 0.4
Leu308Val	78 ± 9 (13)	14 ± 2 (3)
Leu308Ala	2790 ± 300 (473)	113 ± 12 (27)

[a] The inhibition patterns were competitive with respect to the substrate *S*-tetralol. K_i ratio of MT/WT is given in parenthesis.

The above results illustrate the role of the bulky side-chain of Leu308 in inhibitor binding through the formation of important van der Waals contacts with the DCL and BPSA molecules (Fig. 2). The effect resulting from shortening the side-chain of Leu308 on inhibitor binding was reflected in the K_i values where the inhibition potency decreased for the mutants as the side-chain shortened from leucine to valine to alanine. In the Leu308Ala MT the alanine side-chain was not present within van der Waals contacts from the inhibitor, resulting in higher K_i values than those of the Leu308Val MT. Furthermore, the K_i values for DCL in comparison with those for BPSA, showed that the mutations of Leu308 had a lesser impact on the binding of BPSA than for DCL. This effect is likely due to the additional van der Waals contacts made by the phenyl ring of BPSA

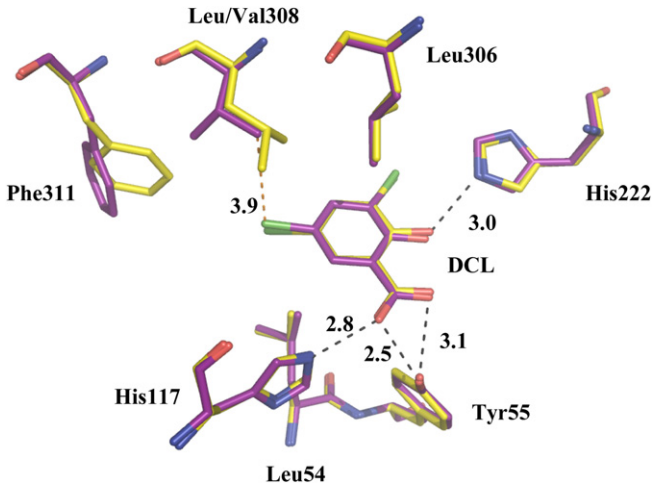

Fig. 1. Superimposition of the crystal structures of the WT AKR1C1 (yellow) and the Leu308Val MT (purple) with DCL bound in the active site. Shortest distance between DCL and residue Val308 (orange dotted lines) and hydrogen bonds with the catalytic residues (black dotted lines) are given in angstroms. (For interpretation of the references to colour in this figure legend, the reader is referred to the web version of this article).

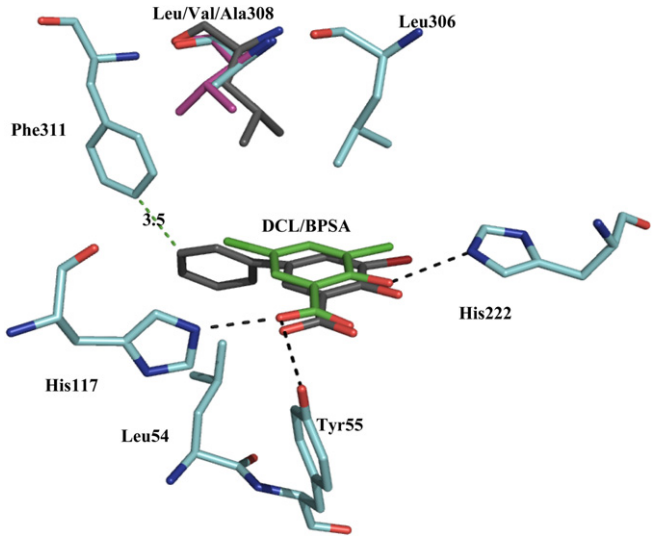

Fig. 2. Docked inhibitors DCL (green) and BPSA (grey) in the active site of AKR1C1 Leu308Ala MT (cyan) with Leu308 WT (grey) and Leu308Val MT (purple) superimposed. Both inhibitors formed conserved hydrogen bonds with the catalytic residues (black dotted lines). The 5-phenyl ring of BPSA extended deeper into the binding site interacting with Phe311 (green dotted lines). (For interpretation of the references to colour in this figure legend, the reader is referred to the web version of this article).

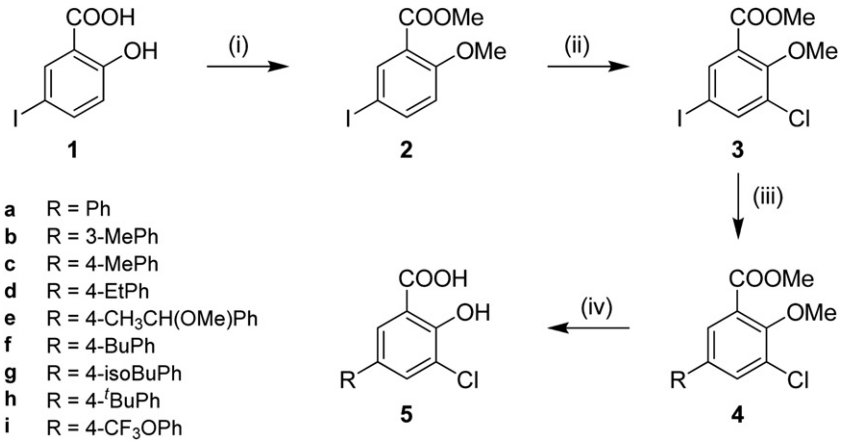

Scheme 1. Synthesis scheme for prepration of compounds **5a–c and 5e–i**. Reagents and conditions: (i) MeI, K_2CO_3, acetone, 96%; (ii) SO_2Cl_2, CH_2Cl_2, 96%; (iii) R–$B(OH)_2$, $PdCl_2(PPh_3)_2$, K_3PO_4, DMF (for **4a–d** and **4f–i**); (iv) BBr_3, CH_2Cl_2.

which extended deeper into the selectivity pocket interacting with the phenyl ring of Phe311 (Fig. 2).

2.3. Synthesis of 5-substituted 3-chlorosalicylic acid derivatives

In our attempts to optimize inhibitor potency and selectivity, 5-substituted 3-chlorosalicylic acid derivatives were prepared using the synthetic approach depicted in Scheme 1. 5-Iodosalicylic acid (**1**) was protected and chlorinated in high yield to give the key intermediate **3**. A range of phenyl substituents were then introduced into the 5-position via Suzuki–Miyaura coupling with the appropriate phenyl boronic acid (compounds **4a–d** and **4f–i**). The final step in the synthesis was the simultaneous deprotection of the methyl ester and methyl ether moieties using boron tribromide, as reported in our earlier study [38]. In general the corresponding salicylic acid derivative **5** was formed in good yield. However, the BBr_3 mediated deprotection of the 5-(4-ethylphenyl) substituted derivative **4d** produced an unexpected product. In this case, the major product was 5-chloro-4-hydroxy-4′-(1-methoxyethyl)biphenyl-3-carboxylic acid (**5e**), which presumably resulted from benzylic bromination and methoxy substitution of the 5-(4-ethylphenyl) group (Scheme 1).

3-Fluoro-5-phenylsalicylic acid (**9**) was prepared using the synthetic approach shown in Scheme 2. This synthesis was based on the approach developed by Micklatcher and Cushman for the preparation of 3-fluorosalicylic acid [41]. Briefly, 3-fluoro-4-methoxybiphenyl (**6**) was O-demethylated using boron tribromide to give the phenol **7**. A Duff reaction, which introduces a formyl group using hexamethylenetetramine (HMT), afforded the salicylaldehyde **8** which was subsequently oxidized to 3-fluoro-5-phenylsalicylic acid (**9**) (Scheme 2).

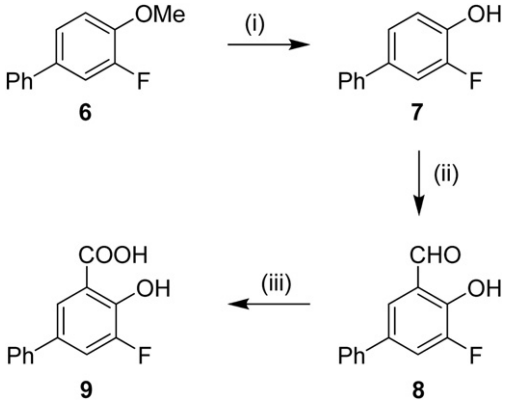

Scheme 2. Synthesis scheme for preparation of compound **9**. Reagents and conditions: (i) BBr_3, CH_2Cl_2, 88%; (ii) hexamethylenetetramine, TFA, H_2SO_4, 41%; (iii) $NaClO_2$, sulfamic acid, $NaH_2PO_4 \cdot H_2O$, dioxane/H_2O, 61%.

2.4. Structure–activity relationships

We have previously reported that 3,5-dihalosalicylic acids are potent AKR1C1 inhibitors, with the 3,5-dichloro analog (i.e. DCL) being the most potent in this series [38,39]. A 5-phenyl substituent was introduced to target a selectivity pocket in the active site of AKR1C1 lined by the three non-polar residues Leu54, Leu308, and Phe311 [38]. BPSA proved to be a potent inhibitor with a K_i value of 4.1 nM and 21-fold selectivity for the AKR1C1 relative to AKR1C2 (Table 3), where the selectivity pocket differs by one amino acid residue (Leu54 in AKR1C1 and Val54 in AKR1C2).

In the present study, the combination of a 3-chloro and a 5-phenyl group (**5a**) afforded a substantial increase in potency ($K_i = 0.86$ nM) with similar level of selectivity compared to BPSA. The effect of further substitution of the 5-phenyl moiety of **5a** was subsequently explored through the evaluation of the salicylic acid derivatives **5b**, **5c** and **5e–j**. Analogs with 3-methylphenyl (**5b**), 4-methylphenyl (**5c**), 4-butylphenyl (**5f**) and 4-isobutylphenyl (**5g**) groups in the 5-position all proved to be potent AKR1C1

Table 3
K_i values of DCL, BPSA and the 5-substituted 3-chlorosalicylic acids towards AKR1C1 and AKR1C2.

Compound	R	X	K_i (nM)[a]		Ratio[b]
			AKR1C1	AKR1C2	
DCL	Cl	Cl	5.9 ± 0.8	70 ± 2.0	11
BPSA	Ph	Br	4.1 ± 0.4	87 ± 12	21
5a	Ph	Cl	0.86 ± 0.01	21 ± 3	24
5b	3-MePh	Cl	1.3 ± 0.1	17 ± 1	13
5c	4-MePh	Cl	2.6 ± 0.1	63 ± 4	24
5e	4-$CH_3CH(OMe)$Ph	Cl	340 ± 23	3000 ± 120	9
5f	4-BuPh	Cl	2.1 ± 0.2	14 ± 1	7
5g	4-IsoBuPh	Cl	2.0 ± 0.1	29 ± 2	15
5h	4-*tert*-BuPh	Cl	96 ± 5	470 ± 17	5
5i	4-CF_3OPh	Cl	29 ± 2	26 ± 2	0.9
5j	PhC≡C	Cl	64 ± 10	168 ± 40	3
9	Ph	F	1.3 ± 0.1	1.5 ± 0.2	1.2

[a] The inhibition patterns were competitive with respect to the substrate *S*-tetralol. Ratio represents AKR1C2/AKR1C1.
[b] Ratio represents AKR1C2/AKR1C1 K_i values.

inhibitors which exhibited K_i values less than 3 nM. Interestingly, the 5-(3-methylphenyl)salicyclic acid **5b** proved to be twice as potent as the corresponding 4-methylphenyl analog **5c**, but was only around half as selective versus AKR1C2. Substitution of the 5-phenyl moiety with a bulky 4-*tert*-butyl group (**5h**), 4-ethylmethoxy group (**5e**) or a more polar 4-trifluoromethoxy group (**5i**) significantly reduced potency. Finally, replacement of the Cl atom of 3-chloro-5-phenylsalicylic acid (**5a**) with a fluorine atom failed to improve potency (compound **9**; K_i = 1.3 nM) and essentially abolished selectivity.

2.5. Evaluation of inhibitory potency at cellular level

The inhibitory potency of compounds **5a** and **9** was evaluated using bovine aortic endothelial cells that were transfected with the cDNA for AKR1C1. The cells exhibited 10-fold higher *S*-tetralol dehydrogenase activity than that of the control cells transfected with the vector alone, and only the AKR1C1-overexpressed cells efficiently metabolized progesterone into 20α-hydroxyprogesterone in the metabolic analysis using liquid chromatography/mass spectrometry, as described previously for BPSA [38]. Compounds **5a** and **9** inhibited the metabolism of progesterone in the cells, and their dose-response curves are shown in Fig. 3. Compound **5a** showed 92% inhibition at 2 μM and 26% inhibition at 0.01 μM, and its IC_{50} value was 100 nM, while the IC_{50} value for compound **9** was 300 nM. It should be noted that the two compounds did not affect the cell viability up to their concentrations of 10 μM. The IC_{50} values determined at cellular level for the two compounds are lower than that (460 nM) of the previously synthesized inhibitor, BPSA [38], correlating with the K_i values determined in vitro using AKR1C1 (Table 3). This indicates that the difference in the type of halogen atom at the 3-position of the 5-phenylsalicylic acid affects the affinity for the enzyme rather than cell permeability. Thus, the presence of the Cl atom at this 3-position is an important structural requisite for the 5-phenylsalicylic acid as a potent AKR1C1 inhibitor.

3. Conclusions

In summary, in our efforts towards the development of potent AKR1C1 inhibitors we have determined the crystal structure of the Leu308Val MT enzyme in ternary complex with $NADP^+$ and DCL, and examined the effects of the Leu308Val and Leu308Ala mutations on the potency of inhibitor. The effect of shortening of the Leu308 side-chain on inhibitor binding was also investigated by modeling the inhibitors DCL and BPSA in the WT and MT AKR1C1 structures. The modeling results were in agreement with the K_i values where the inhibitor potency for the enzyme decreased as the side-chain shortened from leucine to valine to alanine. Attempts to optimize the inhibitors were then carried out by preparing 5-substituted 3-chlorosalicylic acid derivatives. The most potent compound in the series, 3-chloro-5-phenylsalicylic acid (K_i = 0.86 nM), was 24-fold more selective for AKR1C1 over the structurally similar AKR1C2, and potently inhibited the metabolism of progesterone by AKR1C1 in the cells with an IC_{50} value equal to 100 nM. On the other hand, the replacement of the Cl atom of 3-chloro-5-phenylsalicylic acid with a F atom failed to improve potency and essentially abolished selectivity.

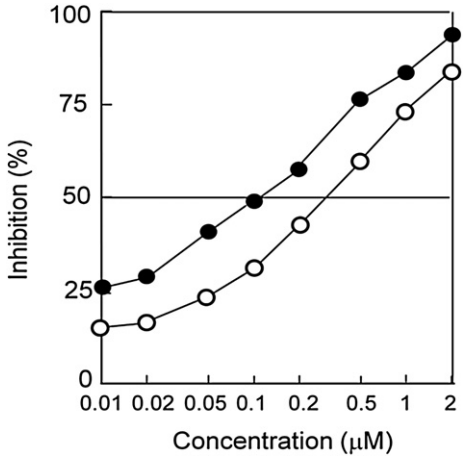

Fig. 3. Dose-response curves for compounds 5a and 9 in the inhibition of progesterone metabolism by the AKR1C1-overexpressed bovine aortic endothelial cells. The cells were cultured for 6 h in the medium containing 30 μM progesterone in the absence (control) or presence of compounds 5a (●) and 9 (○), and the product 20α-hydroxyprogesterone in the media was determined.

4. Experimental section

4.1. Site-directed mutagenesis and purification of recombinant enzymes

Mutagenesis was performed using a QuickChange site-directed mutagenesis kit (Stratagene) and pGEX-2T expression plasmid harbouring cDNA for AKR1C1 as the template [42], according to the protocol described by the manufacturer. The primer pair used for the mutagenesis was composed of sense and antisense oligonucleotides to alter a codon of the AKR1C1 cDNA. The 30-mer primers were synthesized to give the Leu308Val and Leu308Ala mutations. The coding regions of the cDNAs in the expression plasmids were sequenced by using a Beckman CEQ2000XL DNA sequencer in order to confirm the presence of the desired mutation and ensure that no other mutation had occurred. The recombinant WT and MT AKR1C1s and AKR1C2 were expressed in *Escherichia coli* JM109 and purified to homogeneity as previously described [42,43].

4.2. Assay of enzyme activity

The dehydrogenase activities of WT and MT enzymes were determined at 25 °C by measuring the rate of change in NADPH fluorescence (at 455 nm with an excitation wavelength of 340 nm) [21]. The inhibitor was dissolved in methanol and added to the reaction mixture, in which the final concentration of methanol was less than 2.5%. When the fluorescence due to the high concentration of inhibitor interfered with the fluorometric assay, the enzyme activity was determined by measuring the rate of change in NADPH absorbance at 340 nm. The inhibition pattern was determined by fitting the initial velocities using five substrate concentrations ($0.5-5 \times K_m$) in the presence of the three inhibitor concentrations to Lineweaver–Burk and Dixon plots. The K_i value was calculated by using the appropriate programs of the ENZFITTER (Biosoft, Cambridge, UK) and is expressed as the mean ± standard error of at least three determinations.

4.3. Crystallization

Prior to crystallization, AKR1C1 was concentrated to 21 mg/mL in 20 mM HEPES buffer (pH 7.5) with 5 mM 2-mercaptoethanol. A small sample of the enzyme was mixed with $NADP^+$ and the inhibitor dissolved in DMSO (molar ratio of AKR1C1/$NADP^+$/inhibitor was 1:3:3). The final concentration of DMSO did not exceed 2% of the total sample volume. The AKR1C1/$NADP^+$/inhibitor solution was mixed with an equal volume of the crystallization buffer (15% (v/v) polyethylene glycol monomethyl ether 550, 0.01 M zinc sulfate in 0.1 M MES buffer (pH 6.5)). The ternary

complex was crystallized using the hanging drop vapor-diffusion method where 3 μL droplets of the enzyme-buffer solution were placed above a well containing 1 mL of the crystallization solution. Rectangular crystals appeared at 295 K within one week and grew to maximum dimensions of 0.3 × 0.1 × 0.05 mm. The inhibitor DCL (97% purity) was obtained from the Sigma–Aldrich Chemical Co.

4.4. X-ray data collection and structure determination

Crystals of the AKR1C1 Leu308Val MT ternary complex were briefly soaked in the cryo-protecting buffer comprising 0.1 M MES (pH 6.5), 0.01 M zinc sulfate, 20% (v/v) polyglycol monomethyl ether 550 and 30% (v/v) glycerol. The diffraction data were collected at 100 K on a MAR-345 image plate system mounted on a Rigaku RU300 rotating anode generator operating at 50 kV and 90 mA. The X-ray diffraction data were collected to a resolution of 1.9 Å and processed using *HKL2000* and *SCALEPACK* [44]. The structure was solved by the molecular replacement method using the program *MOLREP* in the *CCP4* suite of crystallographic software [45], and the atomic coordinates of AKR1C1 (PDB code 3C3U) without the inhibitor, cofactor and water molecules were used as the search model [39]. The initial model was subjected to iterative cycles of manual fitting into $2F_o-F_c$ and F_o-F_c electron density maps using *Coot* [46], followed by structural refinement using *REFMAC* [47]. The inhibitor molecule, cofactor, waters and zinc ion were added towards the end of the refinement. The atomic coordinates were deposited in the Protein Data Bank (ID code 3GUG).

4.5. Molecular docking

The coordinates for AKR1C1 were obtained from the RCSB Protein Data Bank (ID code 3C3U code). The structure was prepared using the Maestro (Shrödinger, LLC, Portland, OR) software package Version 8.5 where hydrogen atoms in the structure were generated. The Protein Preparation module in Maestro was used to perform a brief relaxation on the starting structure with the "Refinement Only" option, which optimizes the hydroxyl and thiol torsions as well as performing an all-atom constrained minimization to relieve any clashes. The formal charges and appropriate bond orders of the ligands were manually adjusted in Maestro. In order to eliminate any potential bond length and bond angle biases in the structure, the ligands were subjected to a full minimization prior to the docking. The docking calculations were performed using Glide 5.0 on a Linux workstation [48]. A grid box was generated, where the centre of the grid box was defined by the centre of the bound ligand. The calculations were run in the "Extra Precision" (XP) mode of Glide where the ligands were docked flexibly, and to soften the potential for the non-polar parts of the ligands, the van der Waals radius was scaled by 0.8. In order to ensure that the poses generated were conformationally distinct, as well as increasing the diversity of the retained poses, poses with an RMSD less than 0.5 Å and a maximum atomic displacement less than 1.3 Å were discarded as duplicates. All figures for the structural models were prepared by PyMOL (DeLano Scientific, San Carlos, CA, USA).

4.6. Chemistry

Melting points were determined using a Barnstead electrothermal 9100 variable melting point apparatus and are uncorrected. ^{1}H NMR spectra were recorded on a Bruker Avance 300 WB spectrometer. Unless otherwise stated, ^{1}H NMR spectra were obtained in $CDCl_3$ at 300 MHz ^{13}C NMR were recorded on a Varian 600 MHz Inova NMR spectrometer. Unless otherwise stated, ^{13}C NMR spectra were obtained in $CDCl_3$ at 151.4 Hz. Data acquisition and processing was managed using XWINNMR software package version 3.5 and plotting was managed using XWINPLOT software running on the Silicon Graphics workstation. High resolution mass spectra (HRMS) were obtained on Waters LCT Premier XE time-of-flight spectrometer fitted with an electrospray (ESI) ion source and controlled with MassLynx software (version 4.1). Analytical purity was assessed using a Waters 2960 Separation Module coupled with a Waters 998 Photodiode Array Detector with a Phenomax Luna 5u C8 (2) 100A (150 × 4.60 nM ID) column. Samples were run over a gradient of 20–100% Buffer C (20% H_2O, 80% MeOH) in Buffer A (0.1% TFA, 99.9% H_2O) for 10 min followed by isocratic 100% Buffer A for 2 min. In all cases purity was >95%. Thin-layer chromatography was performed on Merck Silica Gel 60 F_{254} plates. 3-Fluoro-4-methoxybiphenyl (**6**) was prepared using the methods described by Mewshaw and co-workers [49].

4.6.1. Methyl 5-iodo-2-methoxybenzoate (*2*)

5-Iodosalicylic acid (5.00 g, 18.93 mmol) was dissolved in acetone (100 mL) and then K_2CO_3 (10.47 g, 75.72 mmol) and MeI (10.75 g, 75.72 mmol) were added. The mixture was refluxed for 48 h, cooled and filtered through Celite. The solvent was removed in vacuo and the residue was redissolved in EtOAc (25 mL), washed with 10% $NaHCO_3$ (15 mL), H_2O (2 × 15 mL) and brine (10 mL), and then dried over $MgSO_4$. The solvent was then evaporated to yield **2** as white crystals (5.32 g, 96%); mp 55–57 °C; ^{1}H NMR δ 8.05 (d, 1H, J = 2.4 Hz), 7.71 (d, 1H, J=2.4, 8.7 Hz), 6.73 (d, 1H, J = 8.7 Hz), 3.68 (s, 6H); ^{13}C NMR δ 165.2, 159.1, 142.1, 140.1, 122.3, 114.5, 81.9, 56.3, 52.4.

4.6.2. Methyl 3-chloro-5-iodo-2-methoxybenzoate (*3*)

Compound **2** (2.00 g, 6.84 mmol) was dissolved in CH_2Cl_2 (10 mL) and then SO_2Cl_2 (2.20 mL, 27.39 mmol) was added over a 5 min period. The solution was then heated to 50 °C and stirred at this temperature for 15 h. The resulting mixture was then cooled, diluted with H_2O (200 mL) and extracted with CH_2Cl_2 (3 × 20 mL). The combined organic layers were washed with brine (10 mL), dried over $MgSO_4$ and concentrated in vacuo. The resulting residue was purified by flash chromatography (0–10% EtOAc/petroleum spirit) to yield beige crystals (2.15 g, 96%); mp 53–54 °C; ^{1}H NMR δ 7.93 (d, 1H, J = 3.3 Hz), 7.79 (d, 1H, J = 3.3 Hz), 3.96 (s, 6H); ^{13}C NMR δ 164.2, 155.8, 143.0, 138.4, 130.7, 128.3, 86.2, 62.0, 52.6.

4.6.3. General procedure for Suzuki–Miyaura coupling of *3* to phenyl derivatives *4a–i*

To a stirred solution of **3** (0.200 g, 618 mmol) in anhydrous DMF (5 mL) were added K_3PO_4 (0.212 g, 1.22 mmol) and the desired boronic acid (1.85 mmol). This solution was then purged with N_2 for 1 h, after which $PdCl_2(PPh_3)_2$ (0.043 g, 0.06 mmol) was added and the reaction was stirred at 70 °C under N_2 overnight. Once the starting material had been consumed (monitored by TLC), the reaction mixture was filtered through SiO_2 by the aid of diethyl ether (25 mL). The organic layer was washed with H_2O (5 × 50 mL), brine (20 mL) and dried over $MgSO_4$. The solvent was removed in vacuo and the residue was purified via flash chromatography (0–10% EtOAc in petroleum ether) to yield the desired product.

*4.6.3.1. Methyl 5-chloro-4-methoxybiphenyl-3-carboxylate (**4a**).* Compound **4a** was prepared using phenyl boronic acid (0.224 g) and **3** (0.200 g) as an amorphous solid (144 mg, 85%). ^{1}H NMR δ 7.92 (d, 1H, J = 2.4 Hz), 7.77 (d, 1H, J = 2.4 Hz), 7.35–7.56 (m, 2H) 7.41 (m, 3H) 3.98 (s, 3H, CH_3) 3.96 (s, 3H, CH_3); ^{13}C NMR δ 166.0, 155.1, 138.6, 138.0, 132.6, 130.1, 129.2, 128.5, 128.2, 127.1, 62.2, 52.7.

*4.6.3.2. Methyl 5-chloro-4-methoxy-3′-methylbiphenyl-3-carboxylate (**4b**).* Compound **4b** was prepared from 3-methylphenyl boronic acid (0.250 g) and **3** (0.200 g) as a brown oil (120 mg, 69%). ^{1}H NMR δ 7.91 (d, 1H, J = 2.4 Hz), 7.76 (d, 1H, J = 2.4 Hz), 7.16–7.36

(m, 4H), 3.98 (s, 3H), 3.96 (s, 3H), 2.42 (s, 3H); ^{13}C NMR δ 166.0, 155.0, 138.8, 138.6, 138.1, 132.6, 130.0, 129.1, 128.9, 128.4, 127.8, 127.02, 124.1, 62.2, 52.7, 21.7.

*4.6.3.3. Methyl 5-chloro-4-methoxy-4′-methylbiphenyl-3-carboxylate (**4c**).* Compound **4c** was prepared from 4-methylphenyl boronic acid (0.250 g) and **3** (0.200 g) as a brown oil (125 mg, 70%). ^{1}H NMR δ 7.89 (d, 1H, J = 2.4 Hz), 7.75 (d, 1H, J = 2.4 Hz), 7.45 (d, 2H, J = 7.9 Hz) 3.97 (s, 3H), 3.95 (s, 3H), 1.58 (s, 3H). ^{13}C NMR δ 165.9, 154.8, 138.0, 137.9, 135.6, 132.2, 129.9, 129.8, 128.1, 127.0, 126.8, 62.1, 52.6, 21.2.

*4.6.3.4. Methyl 5-chloro-4′-ethyl-4-methoxybiphenyl-3-carboxylate (**4d**).* Compound **4d** was prepared from 4-ethylphenyl boronic acid (0.276 g) and **3** (0.200 g) as a brown oil (163 mg, 87%). ^{1}H NMR δ 7.90 (d, 1H, J = 1.6 Hz), 7.75 (d, 1H, J = 1.6 Hz), 7.47 (d, 2H, J = 8.1 Hz), 7.27 (d, 2H, J = 8.1 Hz), 3.95 (s, 3H), 3.97 (s, 3H), 2.69 (q, 2H, J = 7.6 Hz), 1.28 (t, 3H, J = 7.6 Hz); ^{13}C NMR δ 165.8, 154.7, 144.3, 137.8, 135.8, 132.2, 129.8, 128.5, 128.1, 126.8, 126.8, 62.0, 52.5, 28.5, 15.5.

*4.6.3.5. Methyl 4′-butyl-5-chloro-4-methoxybiphenyl-3-carboxylate (**4f**).* Compound **4f** was prepared from 4-butylphenyl boronic acid (0.322 g) and **3** (0.200 g) as a brown oil (183 mg, 89%). ^{1}H NMR δ 7.89 (s, 1H), 7.75 (s, 1H), 7.45 (d, 2H, J = 7.8 Hz), 7.25 (d, 2H, J = 7.8 Hz), 3.96 (s, 3H), 3.94 (s, 3H), 2.64 (t, 2H, J = 7.7 Hz), 1.59–1.67 (m, 2H), 1.31–1.44 (m, 2H), 0.94 (t, 3H, J = 7.4 Hz); ^{13}C NMR δ 166.1, 154.9, 143.2, 138.0, 136.0, 132.4, 130.0, 129.2, 128.3, 127.0, 126.9, 62.2, 52.7, 35.5, 33.8, 22.6, 14.1.

*4.6.3.6. Methyl 5-chloro-4′-isobutyl-4-methoxybiphenyl-3-carboxylate (**4g**).* Compound **4g** was prepared from 4-isobutylphenyl boronic acid (0.327 g) and **3** (0.200) as a brown oil (155 mg, 76%). ^{1}H NMR δ 7.91 (d, 1H, J = 2.4 Hz), 7.76 (d, 1H, J = 2.4 Hz), 7.46 (d, 2H, J = 8.0 Hz), 7.22 (d, 2H, J = 8.0 Hz), 3.97 (s, 3H), 3.95 (s, 3H), 2.51 (d, 2H, J = 7.2 Hz), 1.85–1.94 (m, 1H), 0.93 (d, 6H, J = 6.6 Hz); ^{13}C NMR δ 166.1, 154.9, 141.9, 138.0, 136.0, 132.4, 130.0, 129.9, 128.3, 127.0, 126.8, 62.2, 52.7, 45.2, 30.4, 22.5.

*4.6.3.7. Methyl 4′-tert-butyl-5-chloro-4-methoxybiphenyl-3-carboxylate (**4h**).* Compound **4h** was prepared from 4-*tert*-butylphenyl boronic acid (0.328 g) and **3** (0.200 g) as a brown oil (149 mg, 90%). ^{1}H NMR δ 7.91 (d, 1H, J = 2.4 Hz), 7.76 (d, 1H, J = 2.4 Hz), 7.45–7.48 (m, 4H), 3.97 (s, 3H), 3.95 (s, 3H), 1.35 (s, 9H); ^{13}C NMR δ 166.1, 154.9, 151.4, 137.9, 135.8, 132.5, 130.0, 128.3, 127.1, 126.8, 126.2, 62.3, 52.7, 34.8, 31.5.

*4.6.3.8. Methyl 5-chloro-4-methoxy-4′-(trifluoromethoxy)biphenyl-3-carboxylate (**4i**).* Compound **4i** was prepared from 4-trifluoromethoxyphenyl boronic acid (0.378 g) and **3** (0.200 g) as a brown oil (135 mg, 61%). ^{1}H NMR δ 7.87 (d, 1H, J = 2.4 Hz), 7.72 (d, 1H, J = 2.4 Hz), 7.56 (m, 2H), 7.28 (m, 2H), 3.96 (s, 6H); ^{13}C NMR δ 165.6, 155.3, 149.1, 137.2, 136.4, 132.3, 130.1, 128.3, 128.2, 127.1, 121.4, 120.4 (J = 256 Hz), 62.1, 52.6.

*4.6.4. General procedure for demethylation of compounds **4a–i***

To a stirred solution of the appropriate carboxylate **4** in CH_2Cl_2 (3 mL) at −78 °C under N_2 BBr_3 (10 equiv.) in CH_2Cl_2 was added over a 5 min period. The reaction mixture was stirred overnight at rt and once the starting material had been consumed (as monitored by TLC), the reaction was quenched via the addition of MeOH (10 mL). The solvent was removed in vacuo to give a crude solid, which was then treated by repeated addition and evaporation of MeOH (5 × 5 mL) to remove volatile impurities. H_2O (15 mL) was added and the pH was adjusted to 14. The aqueous layer was washed with EtOAc (3 × 10 mL). The aqueous layer was then collected and acidified to pH 2. The aqueous layer was then extracted with EtOAc (3 × 15 mL). The organic layers were combined and dried over Na_2SO_4. The solvent was removed in vacuo to yield the deprotected product **5**.

*4.6.4.1. 5-Chloro-4-hydroxybiphenyl-3-carboxylic acid (**5a**).* Compound **5a** was obtained as white solid (88 mg, 69%); mp 200–205 °C (dec.); ^{1}H NMR (CD_3OD) δ 7.96 (d, 1H, J = 2.3 Hz), 7.75 (d, 1H, J = 2.3 Hz), 7.22–7.49 (m, 5H); ^{13}C NMR (CD_3OD) δ 173.4, 158.4, 140.3, 135.0, 134.2, 130.3, 128.8, 128.3, 127.7, 123.6, 115.8; HRMS (ESI) m/z calcd for $C_{13}H_9ClO_3$ $[M - H]^-$ 247.0167, found 247.0173.

*4.6.4.2. 5-Chloro-4-hydroxy-3′-methylbiphenyl-3-carboxylic acid (**5b**).* Compound **5b** was obtained from **4d** as a beige solid (78 mg, 90%); mp 205–210 °C (dec.); ^{1}H NMR (CD_3OD) δ 7.83 (d, 1H, J = 2.4 Hz), 7.62 (d, 1H, J = 2.4 Hz), 7.10–7.17 (m, 3H), 6.97–6.99 (m, 1H), 2.22 (s, 3H); ^{13}C NMR (CD_3OD) δ 171.7, 156.6, 138.6, 138.4, 133.4, 132.6, 128.5, 127.8, 126.7, 126.6, 123.2, 121.8, 114.1, 20.1; HRMS (ESI) m/z calcd for $C_{14}H_{11}ClO_3$ $[M - H]^-$ 261.0324, found 261.0321.

*4.6.4.3. 5-Chloro-4-hydroxy-4′-methylbiphenyl-3-carboxylic acid (**5c**).* Compound **5c** was obtained as a beige solid (90 mg, 99%); mp 210–215 °C (dec.); ^{1}H NMR (CD_3OD) δ 8.05 (d, 1H, J = 2.4 Hz), 7.85 (d, 1H, J = 2.4 Hz), 7.44 (d, 2H, J = 7.8 Hz), 7.26 (d, 2H, J = 7.8 Hz), 2.40 (s, 3H); ^{13}C NMR (CD_3OD) δ 173.1, 157.9, 138.5, 137.2, 134.7, 133.9, 130.7, 127.9, 127.4, 123.3, 115.5, 21.1; HRMS (ESI) m/z calcd for $C_{14}H_{11}ClO_3$ $[M - H]^-$ 261.0324, found 261.0327.

*4.6.4.4. 5-Chloro-4-hydroxy-4′-(1-methoxyethyl)biphenyl-3-carboxylic acid (**5e**).* Compound **5e** was obtained as a beige solid (75 mg, 66%); mp 185–190 °C (dec.); ^{1}H NMR (CD_3OD) δ 8.03 (d, 1H, J = 0.9 Hz), 7.82 δ (d, 1H, J = 0.9 Hz), 7.53 (d, 2H, J = 7.6 Hz), 7.37 (d, 2H, J = 7.6 Hz), 4.36 (q, 1H, J = 6.3 Hz), 3.22 (s, 3H), 1.42 (d, 3H, J = 6.3 Hz); ^{13}C NMR (CD_3OD) δ 171.5, 156.1, 142.9, 136.9, 133.2, 131.4, 126.7, 126.5, 126.4, 121.5, 114.9, 78.2, 55.8, 23.5; HRMS (ESI) m/z calcd for $C_{16}H_{15}ClO_4$ $[M - H]^-$ 305.0586, found 305.0597.

*4.6.4.5. 4′-Butyl-5-chloro-4-hydroxybiphenyl-3-carboxylic acid (**5f**).* Compound **5f** was obtained as a beige solid (80 mg, 78%); mp 190–195 °C (dec.); ^{1}H NMR (DMSO-d_6) δ 8.00 (d, 1H, J = 2.4 Hz), 7.79 (t, 1H, J = 2.4 Hz), 7.42 (d, 2H, J = 8.4 Hz), 7.22 (d, 2H, J = 8.4 Hz), 2.62 (t, 2H, J = 7.7 Hz), 1.56–1.66 (m, 2H), 1.31–1.43 (m, 2H), 0.94 (t, 3H, J = 7.4 Hz); ^{13}C NMR (DMSO-d_6) δ 171.5, 155.9, 141.8, 135.2, 133.1, 131.7, 129.0, 126.4, 126.2, 121.4, 114.8, 34.3, 33.0, 21.7, 13.7; HRMS (ESI) m/z calcd for $C_{17}H_{17}ClO_3$ $[M - H]^-$ 303.0793, found 303.0789.

*4.6.4.6. 5-Chloro-4-hydroxy-4′-isobutylbiphenyl-3-carboxylic acid (**5g**).* Compound **5g** was obtained as a beige solid (114 mg, 98%); mp 175–180 °C (dec.); ^{1}H NMR (CD_3OD) δ 8.05 (d, 1H, J = 2.4 Hz), 7.85 (d, 1H, J = 2.4 Hz), 7.49 (d, 2H, J = 7.9 Hz), 7.24 (d, 2H, J = 7.9 Hz), 2.52 (d, 2H, J = 6.9 Hz), 1.92 (m, 1H) 0.93 (t, 6H, J = 6.2 Hz); ^{13}C NMR (CD_3OD) δ 173.2, 157.9, 142.3, 137.5, 134.6, 133.9, 130.8, 127.9, 127.2, 123.3, 115.6, 46.0, 31.5, 22.7; HRMS (ESI) m/z calcd for $C_{17}H_{17}ClO_3$ $[M - H]^-$ 303.0793, found 303.0804.

*4.6.4.7. 4′-tert-Butyl-5-chloro-4-hydroxybiphenyl-3-carboxylic acid (**5h**).* Compound **5h** was obtained as a beige solid (130 mg, 90%); mp 215–220 °C (dec.); ^{1}H NMR (CD_3OD) δ 8.03 (s, 1H), 7.81 (s, 1H), 7.47 (br s, 4H), 1.35 (s, 9H); ^{13}C NMR (CD_3OD) δ 171.6, 156.5, 150.2, 135.6, 133.2, 132.3, 126.4, 125.7, 125.5, 121.9, 33.9, 30.3; HRMS (ESI) m/z calcd for $C_{17}H_{17}ClO_3$ $[M - H]^-$ 303.0793, found: 303.0787.

*4.6.4.8. 5-Chloro-4-hydroxy-4′-(trifluoromethoxy)biphenyl-3-carboxylic acid (**5i**).* Compound **5i** was obtained as a beige solid (91 mg, 98%); mp 220–225 °C (dec.); ^{1}H NMR (CD_3OD) δ 8.00 (d, 1H,

$J = 2.4$ Hz), 7.65 (d, 1H, $J = 2.4$ Hz), 7.59 (d, 2H, $J = 8.6$ Hz), 7.24 (d, 2H, $J = 8.6$ Hz); ^{13}C NMR (CD_3OD) δ 173.1, 157.4, 148.2, 138.7, 131.0, 129.5, 127.5, 127.0, 121.4, 121.0, 120.6 (q, $J = 259$ Hz), 119.3; HRMS (ESI) m/z calcd for $C_{14}H_8ClF_3O_4$ $[M - H]^-$ 330.9990, found: 330.9994.

4.6.5. 3-Fluorobiphenyl-4-ol (**7**)

To a stirring solution of **6** (0.42 g, 2.1 mmol) in CH_2Cl_2 (5 mL) at −78 °C was added dropwise BBr_3 (2.81 mL, 16.5 mmol) over 5 min. The reaction mixture was stirred overnight at rt. Once all starting material had been consumed (as monitored by TLC), the reaction mixture was quenched via the dropwise addition of MeOH (5 mL). The solvent was removed in vacuo to yield a brown solid. This crude mixture was then purified via flash chromatography (0–8% Et_2O in petroleum ether) to yield solid white needles (0.338 g, 88%); mp 80–85 °C (dec.); ^{1}H NMR δ 7.52 (d, 2H, $J = 7.5$ Hz), 7.42 (t, 2H, $J = 7.3$ Hz), 7.31 (m, 3H), 7.10 (t, 1H, $J = 8.6$ Hz, 1H).

4.6.6. 5-Fluoro-4-hydroxybiphenyl-3-carbaldehyde (**8**)

To a solution of **7** (0.320 g, 1.7 mmol) in CF_3CO_2H (5 mL) was added portion wise, hexamethylenetetramine (0.477 g, 3.4 mmol) over a 10 min period. The solution was refluxed for 14 h, cooled and poured into H_2O (30 mL). A solution of 50% H_2SO_4 (15 mL) was then added and the solution was stirred for 2 h at rt. The solution was then extracted with EtOAc (3 × 20 mL) and the combined organic extracts were washed with 1 M HCl (5 × 10 mL), brine (20 ml), dried over $MgSO_4$ and concentrated in vacuo. The resulting yellow oil was purified using flash chromatography (0–50% CH_2Cl_2 in petroleum ether) to yield a yellow solid (0.152 g, 41%); mp 55–59 °C (dec.); ^{1}H NMR ($CDCl_3$) δ 10.96 (s, 1H), 10.01 (s, 1H), 7.36–7.63 (m, 6H); ^{13}C NMR ($CDCl_3$) δ 196.4, 151.1 (d, $J = 250$ Hz), 148.9 (d, $J = 12.7$ Hz), 138.3, 133.4, 133.5, 129.1, 127.9, 126.6, 122.4, 121.5 (d, $J = 18.5$ Hz).

4.6.7. 5-Fluoro-4-hydroxybiphenyl-3-carboxylic acid (**9**)

To a stirred solution of **8** (0.140 g, 0.65 mmol) in 1,4-dioxane (3 mL) and H_2O (1 mL) was added sulfamic acid (0.094 g, 0.97 mmol) and $NaH_2PO_4 \cdot H_2O$ (0.390 g, 2.58 mmol). The mixture was cooled in an ice-bath for 15 min and a solution of $NaClO_2$ (0.076 g, 0.84 mmol) in H_2O (1 mL) was added dropwise to the mixture, and the solution was stirred for an additional 15 min. Na_2SO_3 (0.098 g, 0.78 mmol) was then added and stirring was continued for an additional 15 min. The solution was then acidified to pH 1 by dropwise addition of conc. HCl and the solution was extracted with EtOAc (3 × 10 mL). The organic layers were combined and washed with H_2O (20 mL) and dried over $MgSO_4$. The solvent was removed in vacuo and the crude residue was purified by flash chromatography (0–10% MeOH in CH_2Cl_2) to yield a white solid (0.092 g, 61%); mp 213–215 °C (dec.); ^{1}H NMR (CD_3OD) δ 7.80 (s, 1H), 7.53–7.63 (m, 3H), 7.41 (br t, 2H), 7.31 (br t, 1H); ^{13}C NMR (CD_3OD) δ 173.1152.9 (d, $J = 246$ Hz), 150.9 (d, $J = 13.8$ Hz), 140.2, 133.2, 130.1, 128.6, 127.6, 124.5, 120.7 (d, $J = 18.5$ Hz), 116.4; HRMS (ESI) m/z calcd for $C_{13}H_9FO_3$ $[M - H]^-$ 231.0463, found: 231.0459.

4.7. Evaluation of inhibitors in the cells

Bovine aortic endothelial cells, a generous gift from Taisho Pharmaceutical Co. (Saitama, Japan), were cultured in Dulbecco's modified Eagle medium supplemented with 10% fetal bovine serum, penicillin (100 U/mL) and streptomycin (100 μg/mL) at 37 °C in a 5% CO_2 incubator. In all experiments, the cells were used at passages 4–8, and the endothelial cobblestone morphology was confirmed microscopically before use. The eukaryotic expression vector pGW1 harbouring the cDNA for AKR1C1 was constructed and transfected into sub-confluent bovine aortic endothelial cells using the Lipofectamine 2000 (Invitrogen) as described previously [38]. The transfected cells were maintained in the medium without fetal bovine serum for 2 h, and then used to evaluate the inhibitory effects of compounds **5a** and **9** on the metabolism of progesterone in the cells. The cells were pretreated for 2 h with various concentrations of inhibitors prior to incubating for 6 h with 30 μM progesterone. The metabolite, 20α-hydroxyprogesterone, in the culture media was extracted twice by ethyl acetate, and quantified on an LC/MS using a Chiralcel OJ-H 5 μ column as described previously [19].

Acknowledgements

UD is the recipient of a Monash Graduate School postgraduate scholarship. This work was partly supported by a Grant-in-Aid for Young Scientists (to SE).

References

[1] T.M. Penning, Endocr. Rev. 18 (1997) 281–305.
[2] T.M. Penning, Hum. Reprod. Update 9 (2003) 193–205.
[3] B. Persson, Y. Kallberg, J.E. Bray, E. Bruford, S.L. Dellaporta, A.D. Favia, R.G. Duarte, H. Jörnval, K.L. Kavanagh, N. Kedishvili, M. Kisiela, E. Maser, R. Mindnich, S. Orchard, T.M. Penning, J.M. Thornton, J. Adamski, U. Oppermann, Chem. Biol. Interact. 178 (2009) 94–98.
[4] J.M. Jez, T.M. Penning, Chem. Biol. Interact. 130–132 (2001) 499–525.
[5] O.A. Barski, S.M. Tipparaju, A. Bhatnagar, Drug Metab. Rev. 40 (2008) 553–624.
[6] J.M. Jez, M.J. Bennett, B.P. Schlegel, M. Lewis, T.M. Penning, Biochem. J. 326 (1997) 625–636.
[7] G. Sanli, J.I. Dudley, M. Blaber, Cell Biochem. Biophys. 38 (2003) 79–101.
[8] T.M. Penning, Y. Jin, V.V. Heredia, M. Lewis, J. Steroid Biochem. Mol. Biol. 85 (2003) 247–255.
[9] L.J. Askonas, J.W. Ricigliano, T.M. Penning, Biochem. J. 278 (1991) 835–841.
[10] B.P. Schlegel, J.M. Jez, T.M. Penning, Biochemistry 37 (1998) 3538–3548.
[11] C.E. Grimshaw, K.M. Bohren, C.J. Lai, K.H. Gabbay, Biochemistry 34 (1995) 14356–14365.
[12] B. Nidetzky, M. Klimacek, P. Mayr, Biochemistry 40 (2001) 10371–10381.
[13] T.M. Penning, M.E. Burczynski, J.M. Jez, C.F. Hung, H.K. Lin, H. Ma, M. Moore, N. Palackal, K. Ratnam, Biochem. J. 351 (2000) 67–77.
[14] D.R. Bauman, S. Steckelbroeck, T.M. Penning, Drug News Perspect. 17 (2004) 563–578.
[15] T.M. Penning, Y. Jin, T.L. Rizner, D.R. Bauman, Mol. Cell. Endocrinol. 281 (2008) 1–8.
[16] W.C. Cooper, Y. Jin, T.M. Penning, J. Biol. Chem. 282 (2007) 33484–33493.
[17] S. Steckelbroeck, Y. Jin, S. Gopishetty, B. Oyesanmi, T.M. Penning, J. Biol. Chem. 279 (2004) 10784–10795.
[18] Y. Jin, T.M. Penning, Biochemistry 45 (2006) 13054–13063.
[19] S. Ishikura, S. Nakajima, T. Kaneko, S. Shintani, N. Usami, I. Yamamoto, V. Carbone, O. El-Kabbani, A. Hara, in: H. Weiner, B. Plapp, R. Lindahl, E. Maser (Eds.), Enzymology and molecular biology of carbonyl metabolism, vol. 12, Purdue University Press West Lafayette, 2006, pp. 341–351.
[20] Y. Zhang, I. Dufort, P. Rheault, V. Luu-The, J. Mol. Endocrinol. 25 (2000) 221–228.
[21] Y. Higaki, N. Usami, S. Shintani, S. Ishikura, O. El-Kabbani, A. Hara, Chem. Biol. Interact. 143–144 (2003) 503–513.
[22] N. Usami, T. Yamamoto, S. Shintani, S. Ishikura, Y. Higaki, Y. Katagiri, A. Hara, Biol. Pharm. Bull. 25 (2002) 441–445.
[23] R.P. Piekorz, S. Gingras, A. Hoffmeyer, J.N. Ihle, Y. Weinstein, Mol. Endocrinol. 19 (2005) 431–440.
[24] I. Sayeed, D.G. Stein, Prog. Brain Res. 175 (2009) 219–237.
[25] I. Roglio, R. Bianchi, S. Gotti, S. Scurati, S. Giatti, M. Pesaresi, D. Caruso, G.C. Panzica, R.C. Melcangi, Neuroscience 155 (2008) 673–685.
[26] I. Roglio, R. Bianchi, F. Camozzi, V. Carozzi, I. Cervellini, D. Crippa, G. Lauria, G. Cavaletti, R.C. Melcangi, J. Peripher. Nerv. Syst. 14 (2009) 36–44.
[27] E. Leonelli, R. Bianchi, G. Cavaletti, D. Caruso, D. Crippa, L.M. Garcia-Segura, G. Lauria, V. Magnaghi, I. Roglio, R.C. Melcangi, Neuroscience 144 (2007) 1293–1304.
[28] J.J. Lambert, D. Belelli, C. Hill-Venning, J.A. Peters, Trends Pharmacol. Sci. 16 (1995) 295–303.
[29] T. Smuc, N. Hevir, M. Ribic-Pucelj, B. Husen, H. Thole, T.L. Rizner, Mol. Cell. Endocrinol. 301 (2009) 59–64.
[30] T. Smuc, T.L. Rizner, Mol. Cell. Endocrinol. 301 (2009) 74–82.
[31] M.J. Lewis, J.P. Wiebe, J.G. Heathcote, BMC Cancer 4 (2004) 27.
[32] D.C. Seo, J.M. Sung, H.J. Cho, H. Yi, K.H. Seo, I.S. Choi, D.K. Kim, J.S. Kim, A.A. El-Aty, H.C. Shin, Mol. Cancer 6 (2007) 75.
[33] E. Selga, V. Noé, C.J. Ciudad, Biochem. Pharmacol. 75 (2008) 414–426.
[34] C.W. Chien, I.C. Ho, T.C. Lee, Carcinogenesis 30 (2009) 1813–1820.

[35] S. Gobec, P. Brozic, T.L. Rizner, Bioorg. Med. Chem. Lett. 15 (2005) 5170–5175.
[36] M.C. Byrns, S. Steckelbroeck, T.M. Penning, Biochem. Pharmacol. 75 (2008) 484–493.
[37] D.R. Bauman, S.I. Rudnick, L.M. Szewczuk, Y. Jin, S. Gopishetty, T.M. Penning, Mol. Pharmacol. 67 (2005) 60–68.
[38] O. El-Kabbani, P.J. Scammells, J. Gosling, U. Dhagat, S. Endo, T. Matsunaga, M. Soda, A. Hara, J. Med. Chem. 52 (2009) 3259–3264.
[39] U. Dhagat, S. Endo, R. Sumii, A. Hara, O. El-Kabbani, J. Med. Chem 51 (2008) 4844–4848.
[40] G.N. Ramachandran, V. Sasisekharan, Adv. Protein Chem. 23 (1968) 283–438.
[41] M.L. Micklatcher, M. Cushman, Synthesis (1999) 1878–1880.
[42] K. Matsuura, A. Hara, Y. Deyashiki, H. Iwasa, T. Kume, S. Ishikura, H. Shiraishi, Y. Katagiri, Biochem. J. 336 (1998) 429–436.
[43] H. Shiraishi, S. Ishikura, K. Matsuura, Y. Deyashiki, M. Ninomiya, S. Sakai, A. Hara, Biochem. J. 334 (1998) 399–405.
[44] Z. Otwinowski, W. Minor, Meth. Enzymol. 276 (1997) 307–326.
[45] National Collaborative Computational Project, Acta Crystallogr. D Biol. Crystallogr. 50 (1994) 760–763.
[46] P. Emsley, K. Cowtan, Acta Crystallogr. D Biol. Crystallogr. 60 (2004) 2126–2132.
[47] G.N. Murshudov, A.A. Vagin, E.J. Dodson, Acta Crystallogr. D Biol. Crystallogr. 53 (1997) 240–255.
[48] R.A. Friesner, J.L. Banks, R.B. Murphy, T.A. Halgren, J.J. Klicic, D.T. Mainz, M.P. Repasky, E.H. Knoll, M. Shelley, J.K. Perry, D.E. Shaw, P. Francis, P.S. Shenkin, J. Med. Chem. 47 (2004) 1739–1749.
[49] R.J. Edsall Jr., H.A. Harris, E.S. Manas, R.E. Mewshaw, Bioorg. Med. Chem. 11 (2003) 3457–3474.